scientific reports

Check for updates

OPEN

Numerical simulation and experimental validation of the oleogel formation from grape seed oil and beeswax

Zohreh Baratian Ghorghi[1,2], Ali Faezian[3]✉, Samira Yeganehzad[1]✉, Mohammad Ali Hesarinejad[1], Alireza Sheikhi Darani[4], Marcello Fidaleo[2] & Hashem Ahmadi Tighchi[5]

This study focuses on numerical modeling of the oleogelation process using grape seed oil and beeswax and its validation using experimental approach. The main goal is to investigate how the cooling rate affects this process. The necessary physical and thermal properties of the oleogel for modeling were determined through experiments. Additionally, differential scanning calorimetry was used to characterize phase transitions. The apparent heat capacity method was applied in the numerical modeling to simulate the phase change process, and the energy equation was solved using the finite element method. The numerical model demonstrated a maximum relative error of 5.4%, indicating a strong agreement between the numerical results and experimental data. After validating the numerical model, five different cooling rates were investigated. The findings showed that oleogelation begins near the bottom boundary of the setup and then propagates toward the center. Furthermore, the fraction of the total time required for the phase change to complete varied between 0.35 and 0.04 as the cooling rate decreased. This indicates that slower cooling rates provide more time for heat transfer, allowing for more thorough gelation and completing the phase transition in a smaller fraction of the total time. The proposed model can save time and costs while delivering accurate data on creating a beneficial oleogel.

Keywords Numerical simulation, Oleogelation, Grape seed oil, Beeswax, Cooling rate

List of symbols

C_{eq}	Equivalent specific heat capacity (J/kg K)
C_L	Latent heat distribution (J/kg K)
C_p	Specific heat capacity (J/kg K)
D	Container's diameter (m)
H	Specific enthalpy (J/kg)
h	Convection heat transfer coefficient (W/m^2 K)
k	Thermal conductivity (W/m K)
k_a	Thermal conductivity of air (W/m K)
k_c	Thermal conductivity of container (W/m K)
L	Latent heat (J)
Nu_D	Nusselt number
Pr	Prandtl number
Pr_s	Prandtl number at surface temperature
Re_D	Reynolds number

[1]Department of Food Sensory and Cognitive Science, Research Institute of Food Science and Technology (RIFST), Mashhad, Iran. [2]Department for Innovation in Biological, Agro-Food, and Forest Systems, University of Tuscia, Viterbo, Italy. [3]Research Institute of Food Science and Technology (RIFST), P.O. Box 91895-157-356, Mashhad, Iran. [4]Mechanical Engineering Department, Sharif University of Technology, Tehran, Iran. [5]Mechanical Engineering Department, Faculty of Engineering, Ferdowsi University of Mashhad, Mashhad, Iran. ✉email: a.faezian@rifst.ac.ir; s.yeganehzad@rifst.ac.ir

T	Temperature (°C)
t	Time (s)
th_c	Thickness of container (m)
U	Overall heat transfer coefficient (W/m^2 K)
r, z	Coordinate system (m)
Z	Sample height (m)
α_m	Mass fraction
θ	Phase fraction function
ρ	Density (kg/m^3)
μ	Viscosity (N s/m^2)
∇	Spatial gradient (vector) operator

Subscripts

ph1	Phase1 (solution)
ph2	Phase2 (gel)

The texture of many food products is closely related to the type of fat and oil used in them. It is difficult to formulate food products without solid fats because they provide the necessary structure for the products[1–3]. Therefore, solid fats are widely used in the food industry. Due to their solid state, these are high in saturated or trans fatty acids, linked to cardiovascular disease, diabetes, and other disorders[4]. In last few years, a method known as oleogelation has been employed to solve this problem. Oleogelation is a type of gel-forming process to change liquid oils into a solid-like structure[5]. In this way, the nutritional value of the initial oil remains practically unchanged (rich in unsaturated fatty acids and good for health)[2]. During this process, oil droplets are trapped by a material called oleogelator, which can be of natural or synthetic types, in a three-dimensional gel structure[6]. Thus, the state of oil changes from liquid to solid[4]. Oleogelators can be divided into two groups: low molecular weight and high molecular weight. The first group refers to natural small molecules that self-assemble to form a stable crystalline network that stabilises the oil phase. This process takes place under controlled temperature conditions and is driven by physical interactions between molecules such as hydrogen bonding, hydrophobic interactions, and van der Waals forces. Due to these physical interactions, the structure of oleogels is highly sensitive to shear forces and temperature. This group includes; simple sugars, waxes, fatty acids, carbamates, lecithins, ceramides, monoacylglycerols, diacylglycerols, triacylglycerols, n-alkanes and mixtures of γ-oryzanol and phytosterols[7,8]. The second group of oleogelators consists of macromolecular systems that form three-dimensional networks through physicochemical interactions (hydrogen bonds). Their physicochemical properties and polymeric structure give oleogels better viscoelastic properties, which depend on the molecular weight, concentration, and conformation of the polymer. They include proteins (e.g. β-lactoglobulin), some polymers (e.g. colloidal silica), and polysaccharides (e.g. ethyl cellulose, hydroxypropyl methyl cellulose and alginates)[9]. Oleogels have been utilized in the development of numerous food products, such as dairy, spreads, confectionery, meat products, and, bakery products[10–15].

Grape seed oil is a rich resource of phenolic compounds, unsaturated fatty acids, and vitamins. It plays a significant role in cosmetic, pharmaceutical, and food industry applications. These days, the grape seed oil is popular for consumption as an edible oil because of its pleasant sensory features[16,17]. Also, it is ideal for cooking, frying and making salads[18]. It has been determined that consuming grape seed oil reduces the low-density lipoprotein amount. It increases the amount of high-density lipoprotein as well[18,19]. Moreover, the use of grape seed oil has been proposed to delay the aging process and prevent the happening of some chronic diseases[20,21]. As mentioned above, the production of oleogels requires an oleogelator with the ability to develop a three-dimensional network physically strong enough to entrap oil droplets[22]. Oleogelators are lipid materials with low concentrations restraining bulk liquid oil[23]. Waxes are considered to be a proper oleogelator. Beeswax is an organic compound, indeed it is a secretion from bees of the genus Apis[1][24]. It is capable of acting as an edible gelator (GRAS) for various edible oils like other waxes[25–27].

In the gelation process, heat transfer and temperature distribution, and subsequently, phase change propagation is affected by the cooling rate. The cooling rate is a critical factor in this process; not only the gelation time depends on it but also the cooling rate influences the microstructure and macroscopic properties of the gel[28–33]. Several studies have been performed to investigate the effect of the cooling rate on the gelation process[28,30,34–42]. In previous studies, researchers mainly focused on experimental approaches, while numerical simulations have many advantages and provide useful results. As known, in addition to being time-consuming and expensive, experimental methods may be affected by test conditions and sources of error.

To the best of our knowledge, the tendency to utilize numerical simulations in the food industry has increased recently. However, very little numerical research has been performed in the field of edible oleogels. In this investigation, the gelation of an oleogel prepared from grape seed oil and beeswax was simulated and validated based on the experimental setup using a numerical approach. After that, the effects of the cooling rate were studied by the numerical model. Achieving this goal makes it possible to access results with high accuracy and less cost, time and energy so that it can help the food science experts to improve the quality of products for instance.

[1] Apis mellifera Linnaeus.

Material and methods

Material

To prepare the solution for the experiments, Grape seed oil with high linoleic acid content was purchased from Monini Co. (Umbria, Italy) and beeswax was supplied by Zanburkala Co. (Tehran, Iran). Beeswax contains 35% of wax esters (mainly C50), 24% hydroxy esters, 14% hydrocarbon, 12% diesters, 12% free fatty acids and 3% unknown compounds[19]. Samples made of 20% beeswax and 80% grape seed oil were used to produce oleogel.

Experimental setup and measurements

The cooling rate of 0.666 °C/min (the temperature reduction from 85 to 25 °C during 1.5 h) was considered for the oleogelation process to compare the experimental and numerical results. In order to prepare the initial solution, the oil was heated on a heater to 85 °C; after that, beeswax was poured into it and mixed until the wax melted and dissolved completely[43]. Then the solution was placed into an incubator (KBF 115, BINDER CO, Tuttlingen, Germany) with a predetermined cooling program. The velocity of air flow around the container was measured using an anemometer (AM4201, Lutron, Taiwan), which was used in the calculations of the convection coefficient of heat transfer through the boundaries. In addition, before starting the cooling program, thermocouples were located in specific positions of samples to measure the temperature of those placement points during the cooling implementation. Experimental data were obtained by monitoring and reporting the temperature of the considered points as a function of time during the cooling process. These data were used to validate the numerical method. Figure 1 shows the thermocouple placement inside the sample for experimental measurements during the cooling process. More details of the number of thermocouples for each experiment and the location of them are given in the results validation section.

In numerical simulations, the physical and thermal properties of the sample for both phases are required[44]. The density of samples was measured by using a multi pycnometer (MVP – 5 DC, Quantachrome CO, Boynton Beach, USA). A thermal properties analyzer (DECAGON KD2PRO, METER Group Inc, Pullman, USA) was used to determine the specific heat capacity and the thermal conductivity of samples. The phase transition characterization of the present oleogel was determined using the differential scanning calorimetry technique (model DSC-600, Sanaf Co., Iran). In this measurement, the crystallised samples of oleogel at different cooling rates were evaluated to measure their thermal profile characteristics. The basic and temperature parameters of the DSC were calibrated with a pure tin standard dish. To analyse the melting characteristics, the samples were heated from 25 to 85 °C at a gradient of 5 °C/min. Approximately 20 mg of samples were placed in aluminium pans, covered with aluminium lids and sealed. The reference sample was grapeseed oil (as oleogel has two components, wax and oil, and to check the effect of wax concentration on thermal properties, we should use oil without wax as a reference sample)[27,43].

Numerical simulation procedure

Physical model

The physical problem is illustrated in Fig. 2. In the experiment, the sample was inside a container with a cylindrical geometry and symmetrical conditions around the vertical center line. Therefore, the domain geometry is a two-dimensional (2D) axisymmetric rectangle filled with grape seed oil and beeswax mixture. In this way, the left boundary is the axis of symmetry (center line of the sample). The rest of the boundaries are convection which means heat is transferred by convection through those boundaries. Conduction due to the thickness of the right and bottom walls of the container is considered as thermal resistance, so the overall heat transfer coefficient is used for these boundaries. At the top of the sample up to the edge of the container, there is trapped air, which has a lower velocity compared to the air flow on the bottom surface of the container.

The sample container is located in the incubator, whose fan causes uniform airflow inside the chamber during the cooling process. Therefore, it is possible to model heat transfer from boundaries. The convection heat transfer coefficients h of the top and bottom boundaries were calculated by using the following empirical correlation for flow over a disc-shaped surface[45]:

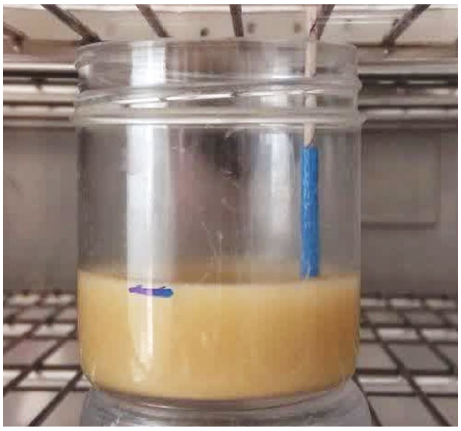

Fig. 1. The placement of the thermocouple inside the sample.

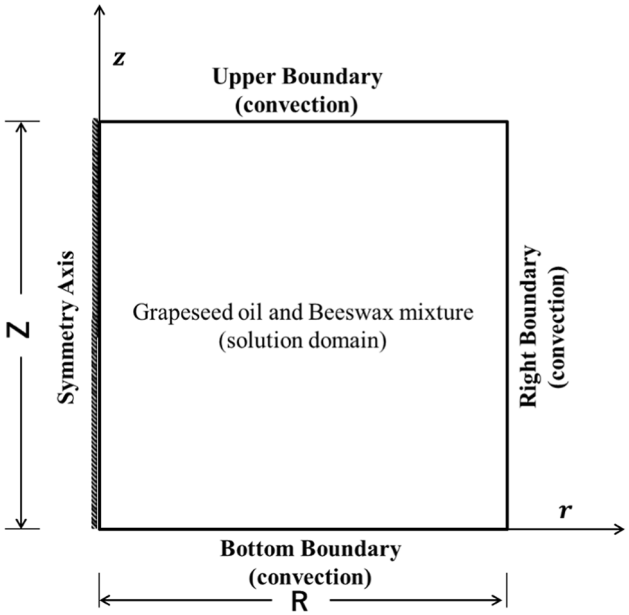

Fig. 2. The Coordinate system and schematic of the physical problem.

$$Nu_D = \frac{hD}{k_a} = 0.356 Re_D^{0.6} Pr^{\frac{1}{3}} \tag{1}$$

where $D = 2R$ is the container diameter, k_a is the thermal conductivity of air, Re_D and Pr are the Reynolds number and the Prandtl number of the surrounding air, respectively. Here, the Reynolds number is defined as $Re = \rho_a V D/\mu_a$, where the diameter of the container D is the characteristic length, ρ_a is the air density, μ_a is the air viscosity, and V is the air velocity around the corresponding boundary, whose values are determined by the mentioned anemometer. Also, the Prandtl number is defined as $Pr = \mu_a C_{p,a}/k_a$, where the specific heat capacity $C_{p,a}$, viscosity μ_a and conduction coefficient k_a are related to air at incubator temperature.

For the right wall, the Zukaskas equation[46] which is used to determine the heat transfer coefficient of a cross-flow around a cylinder, was used:

$$Nu_D = \frac{hD}{k_a} = 0.26 Re_D^{0.6} Pr^{0.37} \left(\frac{Pr}{Pr_s}\right)^{0.25} \tag{2}$$

where Pr_s is the Prandtl number of the surrounding air at the surface temperature of the container. The overall heat transfer coefficients were written as follows to apply the effect of the plastic polymer container on the heat transfer between the ambient and the mixture:

$$for\ bottom\ boundary\ U_b = 1/\left(\frac{1}{h_b} + \frac{th_c}{k_c}\right) \tag{3}$$

$$for\ right\ boundary\ U_r = 1/\left(\frac{1}{h_r} + \frac{r_1 ln\left(\frac{r_2}{r_1}\right)}{k_c}\right) \tag{4}$$

where U is the overall heat transfer coefficient, h is the convection heat transfer coefficient, $k_c = 20 W/mK$ is the conduction heat transfer coefficient of the plastic polymer and $th_c = 1mm$ is container thickness. Also, r_1 and r_2 are inner radius and outer radius of the container, respectively.

Simulation assumptions

The numerical method solves the energy equation considering stagnant fluid inside the domain and obtains the results such as the temperature profile and phase distribution in the sample throughout the oleogelation process. Since the air velocity above the upper surface is too low to cause fluid flow, it is reasonable to assume no flow condition. As mentioned above, a 2D axisymmetric rectangle was considered for the solution domain. The left boundary is considered to be insulated because of the symmetry of the problem and for the rest of the boundary

conditions, Newton's law of cooling is applied using air properties. The radiation heat transfer during the cooling process was assumed negligible.

Governing equations

Phase change occurs when a substance undergoes a change in state on a molecular level. The latent heat is the amount of energy needed to cause phase transition. In this time-dependent study, the apparent heat capacity method was applied to capture the phase change interface[47–50]. In this approach, a single heat transfer equation with effective material properties is solved for both phases. The effect of the phase change enthalpy is taken into account by increasing the temperature-dependent heat capacity during the phase transition[51]. The time-derivative of the enthalpy was calculated as follows[52]:

$$\frac{\partial H}{\partial t} = \frac{\partial H}{\partial T}\frac{\partial T}{\partial t} \tag{5}$$

H is the specific enthalpy of the system, t is the time and T is the temperature.

Instead of applying the effect of latent heat in the energy balance equation exactly when the material reaches its phase change temperature T_{pc}, it was assumed that the phase change takes place in a temperature interval between $T_{pc}-\Delta T/2$ and $T_{pc}+\Delta T/2$. In this interval, the material phase is modeled using a smoothed function, θ, displaying the fraction of phase. For instance, the fraction of phase 1, θ_{ph1}, is equal to 1 for $T \geq T_{pc}+\Delta T/2$ and to 0 for $T \leq T_{pc}-\Delta T/2$. The density, ρ, and the specific enthalpy, H, are defined as follows:

$$\rho = \theta\rho_{ph1} + (1-\theta)\rho_{ph2} \tag{6}$$

$$H = \frac{1}{\rho}(\theta\rho_{ph1}H_{ph1} + (1-\theta)\,\rho_{ph2}H_{ph2}) \tag{7}$$

$\frac{\partial H}{\partial T}$ is the equivalent of specific heat capacity C_p[52–54]. Therefore, the energy equation for this problem can be expressed by:

$$\rho C_{eq}\frac{\partial T}{\partial t} + \nabla \cdot q = Q \tag{8}$$

$$q = -k\nabla T \tag{9}$$

where Q is the additional heat sources which in this case is null and k is the effective thermal conductivity which is represented as follows:

$$k = \theta_{ph1}k_{ph1} + \theta_{ph2}k_{ph2} \tag{10}$$

The equivalent specific heat capacity when the material is in the two-phase region where the material phase is transiting from solution to gel is calculated as below:

$$C_{eq} = \frac{1}{\rho}\left(\theta_{ph1}\rho_{ph1}C_{p,ph1} + \theta_{ph2}\rho_{ph2}C_{p,ph2}\right) + C_L \tag{11}$$

where the indices *ph1* and *ph2* indicate material in phase 1 (solution) or phase 2 (gel), respectively, and C_L is the latent heat distribution which is computed using the following equation:

$$C_L(T) = (H_2 - H_1)\frac{d\alpha_m}{dT} = L\frac{d\alpha_m}{dT} \tag{12}$$

where the mass fraction, α_m, is defined from ρ and θ according to:

$$\alpha_m = \frac{1}{2}\left(\frac{\theta_{ph2}\rho_{ph2} - \theta_{ph1}\rho_{ph1}}{\rho}\right) \tag{13}$$

Overall, the equivalent specific heat capacity in all the regions is defined as below:

$$\begin{cases} C_{eq} = C_{ph1}T & T_{pc} \\ C_{eq} = \frac{1}{\rho}\left(\theta_{ph1}\rho_{ph1}C_{p,ph1} + \theta_{ph2}\rho_{ph2}C_{p,ph2}\right) + C_L & T_{pc} - \frac{\Delta T}{2} \leq T \leq T_{pc} + \frac{\Delta T}{2} \\ C_{eq} = C_{ph2}T & T_{pc} \end{cases} \tag{14}$$

where C_{ph1}, and C_{ph2} are specific heat capacity of solution and gel, respectively.

Boundary conditions at surfaces were expressed as:

$$\text{at right and bottom boundaries}: k\frac{\partial T}{\partial n} = U\left(T - T_\infty\right) \tag{15}$$

Phase	$\rho\left(\frac{\mathrm{kg}}{\mathrm{m}^3}\right)$	$k\left(\frac{\mathrm{W}}{\mathrm{m\,K}}\right)$	$C_p\left(\frac{\mathrm{J}}{\mathrm{kg\,K}}\right)$
Solution	891	0.171	1900
Gel	891	0.22	2428

Table 1. Physical properties of the grape seed oil and beeswax mixture obtained from measurements.

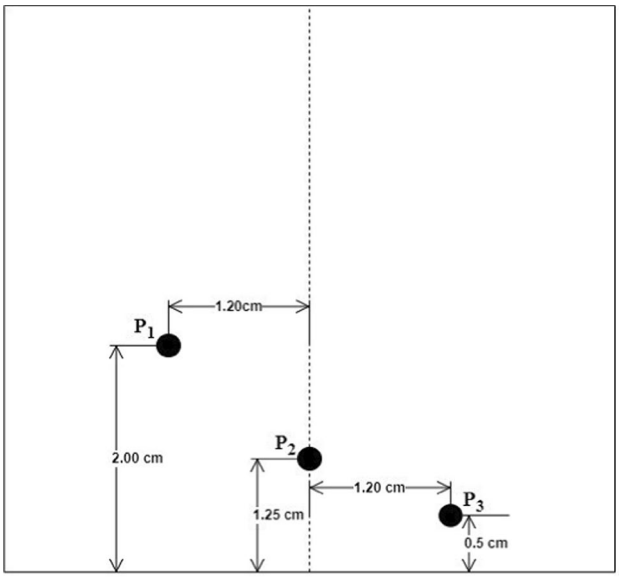

Fig. 3. Positions of thermocouple in the container.

$$\text{at the top boundary}: k\frac{\partial T}{\partial n} = h\left(T - T_\infty\right) \tag{16}$$

$$\text{at the left boundary}: \frac{\partial T}{\partial n} = 0 \tag{17}$$

The properties of the considered mixture in the liquid and gel states, which were determined using the apparatuses mentioned in the experiment method section (section "Experimental setup and measurements"), are presented in Table 1 and used in the numerical simulation. Moreover, from the DSC measurement, the latent heat was determined to be 16,000 J/kg. Also, T_{pc} and ΔT were measured 53.85 °C and 0.8 °C, respectively.

Model implementation, solver settings and convergency

The governing equation was solved numerically using the finite element method. In this method, the quadratic Lagrange scheme was applied for discretization. Streamline diffusion and crosswind diffusion were selected as consistent stabilization methods. A 0.001 relative error was set as the convergency criteria for the time-dependent solver with 1 s time step.

Mesh independency

The mesh independency of the solution was examined by solving the problem for four mesh configurations made of 1380, 3105, 5520, and 8625 cells, respectively. The average temperature–time plots of the domain were compared for the four mesh configurations. The maximum error between the two finer meshes was less than 1%. It can be concluded the mesh with 5520 was the appropriate mesh because there were no noticeable changes in the results with increasing the number of cells. In this way, this grid could provide efficient computing time and sufficient accuracy for results.

Numerical simulation validation

The present numerical model was validated by comparing the simulation results against the experimental data obtained for the oleogelation process of the samples with a cooling rate of 0.666 °C/min. For this purpose, the temperature–time plots from the experiment and the numerical method were compared. In the first experiment, the temperature was measured at three specific positions (P_1, P_2, and P_3) when the sample height was 3.7 cm in the container. The positions of thermocouples are shown in Fig. 3. To conclude that results are independent of the sample mass, the second experiment was conducted with a 1.5 cm sample height in the container and the temperature of the thermocouple at P_3 was used to validate the numerical method.

Figure 4a, 4b, and 4c illustrate the comparison of temperatures for the first experiment (three different points inside the sample). It can be seen from these comparisons that numerical results were consistent with experimental data and the maximum relative error was 5.4%. In both approaches, it was found that the temperature almost remained constant over a range of time. This time range is related to the phase change process that the numerical method has been able to model well. In addition, the results of the second selected experiment (less amount of sample) for validation are presented in Fig. 4d. It was observed that the temperature of the P_3 point obtained from the numerical results was in very good agreement with the results measured in the second experiment so that the maximum relative error was 5.2%. Hence, the proposed numerical approach could be well used for the simulations of the oleogelation process of grape seed oil and beeswax mixture.

Result and discussion

Since the oleogelation phenomenon is inherently transient, in the present study, the various time-dependent results for a specific cooling rate and different cooling rates were examined. It should be mentioned that the temperature reduction around the sample during the cooling was considered from 85 to 25 °C. In numerical simulations, all the runs were taken on core i7 processors, 1.80 GHz, and 8 GB RAM. The maximum CPU time was less than 1 h to provide the converged solution.

Transient behavior of the cooling process

First, the heat transfer inside the sample during the specific cooling process was investigated. For this purpose, Fig. 5 illustrates contours of temperature distribution at different times (18, 36, 50, 54, 68, 72, 81, and 90 min) for a cooling rate of 0.666 °C/min. It was observed that the values related to temperature isotherms decreased over time so that the regions near the right and bottom boundaries had lower temperatures with higher gradients.

This showed that the heat transfer rates of the bottom and right boundaries were higher than the upper boundary because airflow velocity was higher over these boundaries, which caused higher convection heat transfer. Consequently, the gelation process in the middle area near the upper and left boundaries happened after it had occurred in other areas because its temperature decreased with a delay. Similar results were found in an experimental and numerical study about stratification, solidification, and melting[55].

Moreover, it was found from Fig. 5 that the temperature gradient of the solution domain (the number of isotherms) increased over time up to the end of the gelation process, then the number of isotherms decreased and the temperature distribution became more uniform. The reason for this is that during the phase change, the

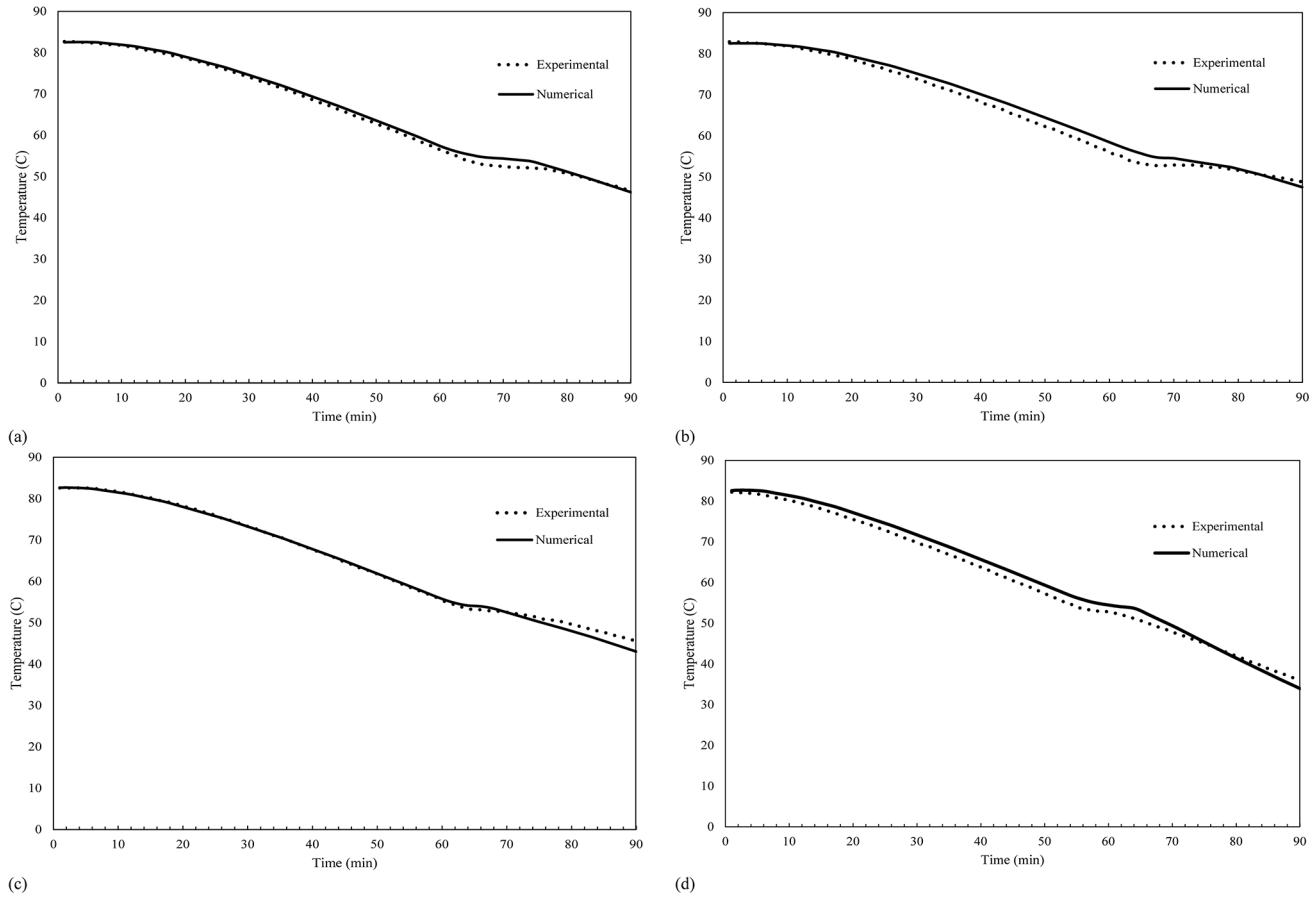

Fig. 4. Comparison of numerical and experimental temperature data: (**a**) at P_1 for the first experiment, (**b**) at P_2 for the first experiment, (**c**) at P_3 for the first experiment and (**d**) at P_3 for the second experiment.

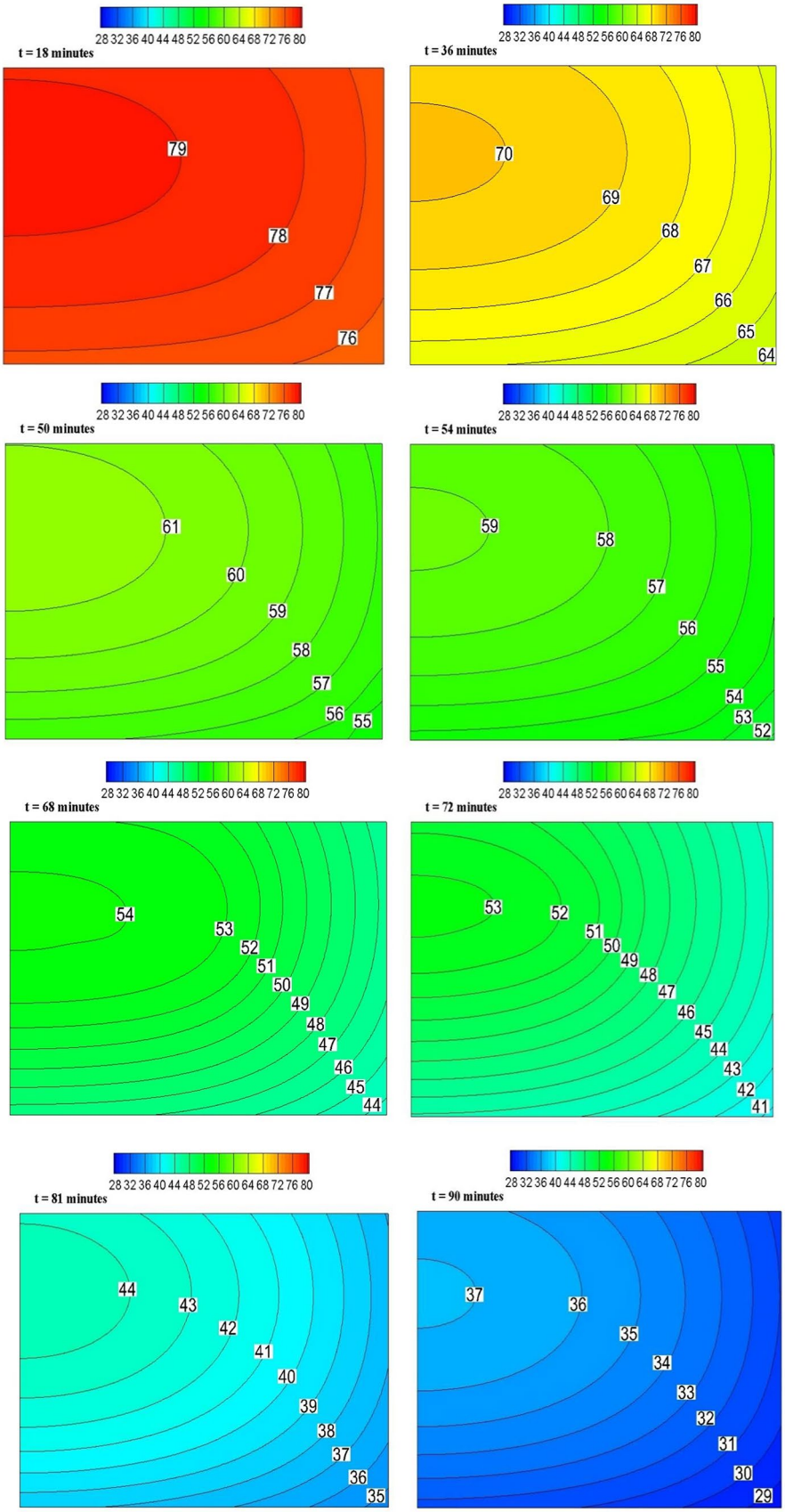

Fig. 5. Temperature contours at different times (18, 36, 50, 54, 68, 72, 81 and 90 min).

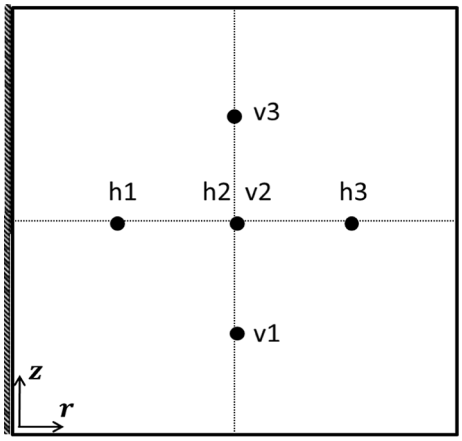

Fig. 6. Schematic of the points located on horizontal and vertical mid-planes.

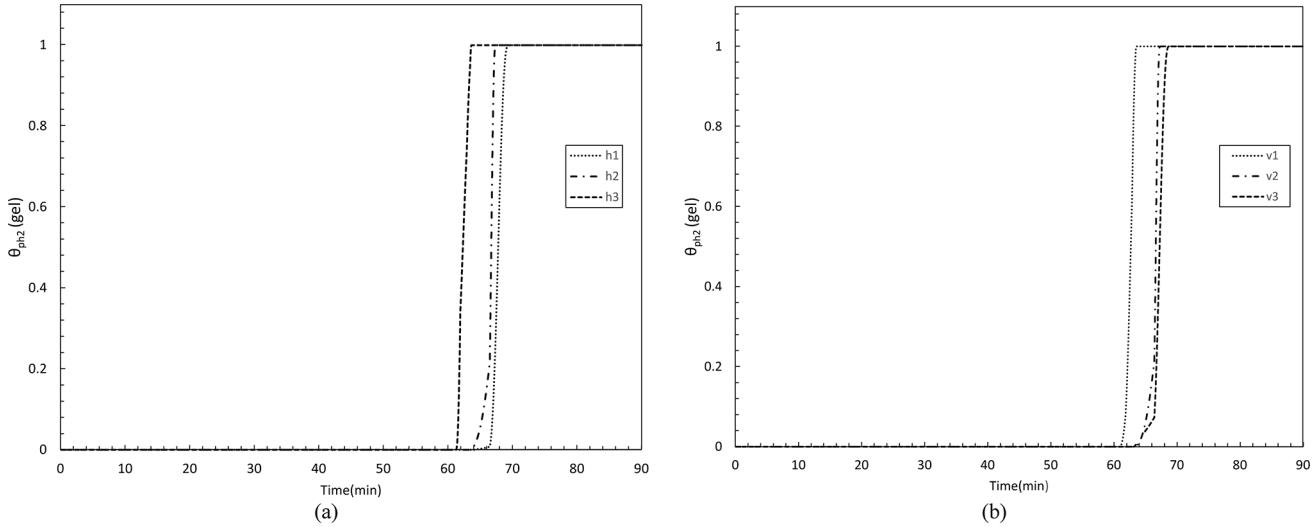

Fig. 7. Phase indication (θ) vs. time for three points located on (**a**) horizontal and (**b**) vertical central lines of the domain.

heat released was allocated to the phase change in each cell of the grid, so the thermal diffusion was reduced, leading to a decrease in the heat transfer between the neighboring points. In fact, in the specific heat capacity relation (Eq. 7), the phase change term was added during gelation, and according to the thermal diffusivity definition, the thermal diffusion decreased along with the increase of the equivalent specific heat capacity. Therefore, the temperature gradient in the solution area increased.

In the phase change phenomenon, the location of the interface between the two phases changes with time as latent heat is absorbed or released at a cell of the domain. This is a critical issue that should be investigated in the problems of oleogel formation. In the present problem, three points with a step of 25% of the corresponding length in the horizontal and vertical central lines of the solution domain were considered to investigate the phase change time. The schematic of the location of the phase change measurement points is represented in Fig. 6. Phase change over time for these points which are located on horizontal and vertical mid-planes is shown in Fig. 7, for a cooling rate of 0.666 °C/min. From Fig. 7a, it can be seen that for the h3 point, which was located on the horizontal mid-plane near the right boundary (wall container), phase change happened earlier than the h2 and h1 points that were away from the right boundary. Also, in Fig. 7b, it can be observed that the phase change began from the point closer to the bottom boundary (v1). These results were consistent with Fig. 5 since the phase change occurred earlier in areas that cooled faster because of higher heat transfer. These findings were also observed in the experiment and are compatible with previous studies[55,56]. As an example, the comparison of the phase contour provided by the numerical method with the image of the experiment after 60 min is presented in Fig. 8. It should be noted that the contour of the numerical method has been obtained from the modeling domain rotation around the axis of symmetry.

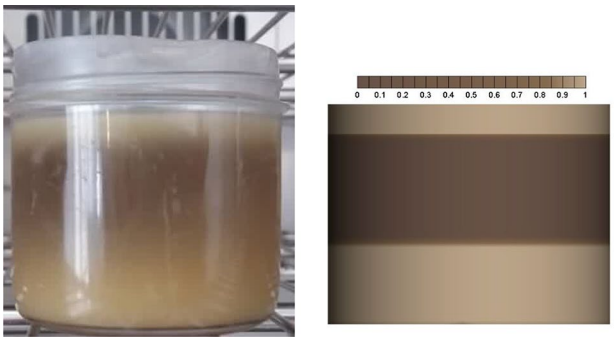

Fig. 8. Comparison of gelation propagation of numerical (right image) and experimental (left image) method after 60 min. The fraction of phase 2 (gel) is plotted on the right image.

Cooling rate effects

In order to investigate the effects of the sample cooling rate, the surrounding air temperature was changed from 85 to 25°C over five different times of 1.5, 3, 6, 12, and 24 h corresponding respectively to cooling rates of 0.666, 0.333, 0.166, 0.083, and 0.041 °C/min. Figure 9 indicates that temperature isotherms were dense in the contours of samples with higher cooling rates. This means that as the cooling time decreased, the temperature gradient in the domain increased. It was because increasing the cooling rate decreased the duration of each step of temperature reduction, resulting in less available time for heat transfer in the domain. This behavior is similar to the behavior of solidification of gelatin hydrogen which was observed in a previous study[44]. However, the contours showed that for all the cooling rates, the domain temperature reached the temperature of the phase change, which led to the phase change in all modes.

Figure 10 illustrates the average temperature of the domain over time for different cooling rates. An almost linear relationship can be observed. Furthermore, it can be seen that the average final temperature of the domain declined as the cooling rate decreased. It is worth mentioning that the final temperature changes in response to changes in the cooling rates decreased at lower rates (less than 0.166 °C/min. For example, by the increment of the cooling time from 1.5 h to 3 h (halving the cooling rate), the average final temperature was reduced by 14.7%. For this finding, it can be argued that low cooling rates allow the domain to have more time for heat transfer to the surroundings. In fact, the heat could transfer more from the convective boundaries into the surrounding cool air. Hence, the average final temperature of samples with slower cooling rates was lower.

Figure 11a and b indicate temperature profiles respectively along the vertical and horizontal mid-lines of the domain for different cooling rates at the end of the process. It can be realized that as the cooling rate increased, temperature and temperature gradient along the mid-line increased. These figures, in agreement with previous figures, showed that in the area in the middle of the sample, with a high cooling rate, the temperature was higher than in other regions, while the samples with a lower cooling rate had more uniform temperatures with lower values.

Numerical simulation results related to phase change for different cooling rates (0.041, 0.083, 0.166, 0.333, and 0.666 °C/min) are given in Table 2. The time for the phase change to reach 50% of the overall domain volume, named equilibrium time and the phase change duration were divided by the total cooling time to properly compare the time-dependent phase change results for each cooling rate. According to Table 2, as the cooling rate increased, the ratio of phase equilibrium time over the total time decreased. Moreover, the phase change duration divided by the corresponding total process duration reduced as the cooling rate decreased. In other words, by reducing the cooling rate (increasing the total cooling time), the formation of oleogel occurred in a smaller fraction of the total time. For example, for cooling with a total time of more than six hours, the equilibrium time of the phases approached 50% of the total time. As previously stated, in cooling processes with lower rates there was more time for heat transfer through the solution domain. So, more cells of the grid medium had time to release latent heat, and phase change occurred earlier. This could be the justification for why the phase change was completed in a shorter time fraction for the slower cooling rate.

Conclusion

The oleogelation prepared from grape seed oil and beeswax was numerically investigated based on an experimental setup during the cooling process. In particular, the numerical model was validated against experimental measurements. Consequently, the corresponding thermophysical properties and experimental conditions of the oleogelation process were used to determine the behavior of oleogel formation at different cooling rates. The transient results showed that the temperature was lower in the areas near the bottom and right boundaries, as a result, the gelation process happened earlier in those areas. Also, it was observed that the cooling time significantly affected the temperature values and the phase transition rate. By reducing the cooling rate, the temperature and the temperature gradient inside the final oleogel decreased because there was enough time for heat transfer. Therefore, the final temperature at the lowest cooling rate was equal to the final temperature of the surroundings, 25 °C. Furthermore, the cooling rate reduction caused a smaller fraction of the total time spent on the phase change. Consequently, the phase change time was reduced from 35% to less than 5% of the corresponding total time and the rest of the time was spent on the reduction of the temperature. Accordingly,

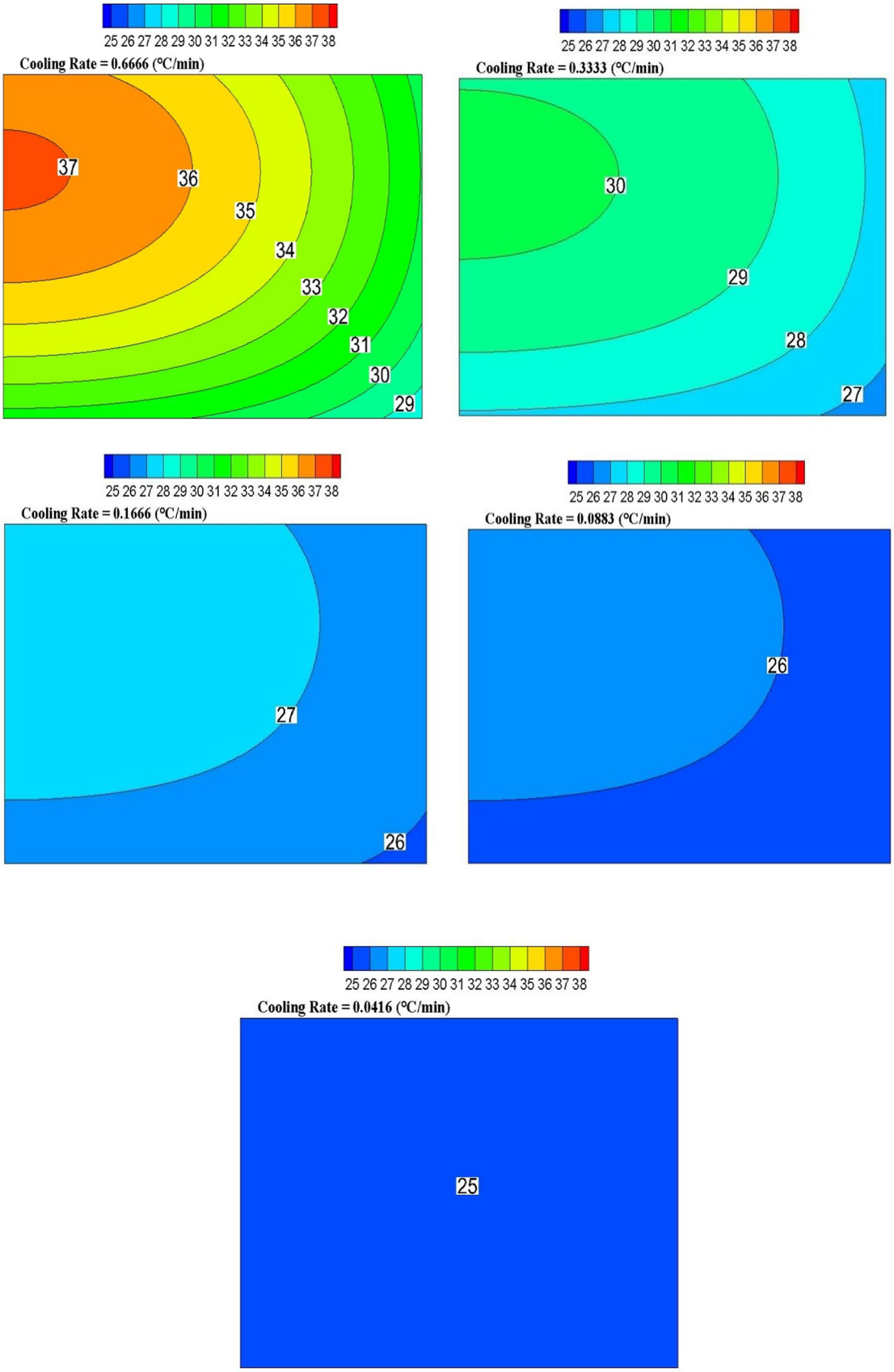

Fig. 9. Final temperature distribution contours for different cooling rates (0.666, 0.333, 0.166, 0.083 and 0.041 °C/min).

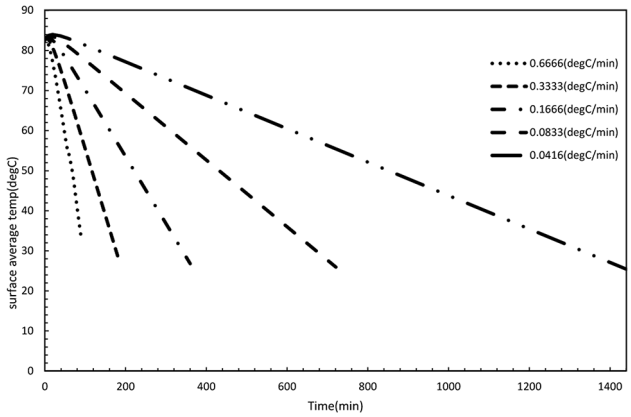

Fig. 10. Average temperature of the solution domain as a function of time for different cooling rates.

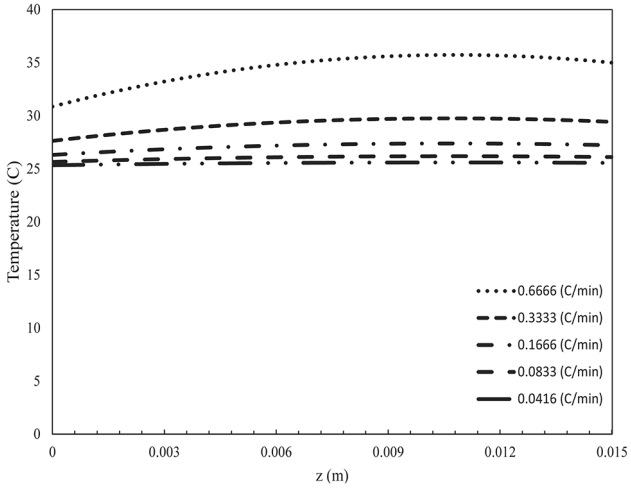

(a)

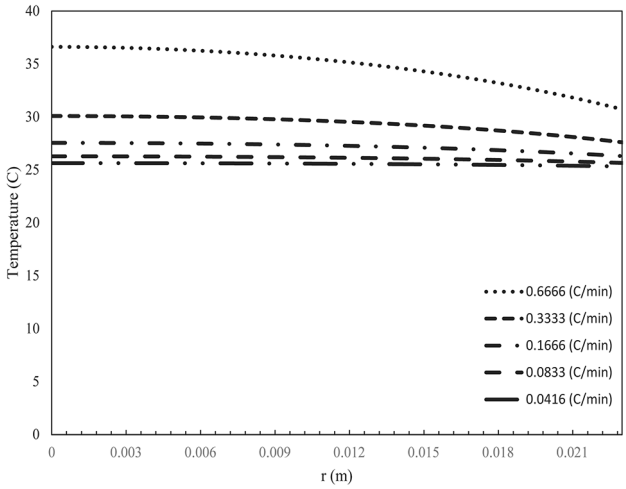

(b)

Fig. 11. Temperature distribution at (**a**) vertical and (**b**) horizontal mid-planes of the domain for different cooling rates.

Cooling rate (°C/min)	Equilibrium time (min)	Phase change start (min)	Phase change finish (min)	Equilibrium time/total time	Phase change time/total time
0.6666	61	50	72	0.68	0.35
0.3333	105	97	111	0.58	0.13
0.1666	199	191	207	0.55	0.08
0.0833	386	375	397	0.53	0.05
0.0416	761	746	777	0.52	0.04

Table 2. Phase change data for different cooling rates.

the proposed model can save costs and time. On the other hand, it provides accurate data on the formation of a beneficial oleogel that can be used in various applications or products, especially in the food industry.

Data availability

All data generated or analyzed during this study are included in this published article.

Received: 3 August 2024; Accepted: 4 December 2024
Published online: 07 January 2025

References

1. Öğütcü, M. & Yılmaz, E. Characterization of hazelnut oil oleogels prepared with sunflower and carnauba waxes. *Int. J. Food Prop.* **18**(8), 1741–1755 (2015).
2. Scharfe, M. & Flöter, E. Oleogelation: From scientific feasibility to applicability in food products. *Eur. J. Lipid Sci. Technol.* **122**(12), 2000213 (2020).
3. Silva, P. M. et al. Oleogels and bigels as alternatives to saturated fats: A review on their application by the food industry. *J. Am. Oil Chem. Soc.* **99**(11), 911–923 (2022).
4. Singh, A., Auzanneau, F. I. & Rogers, M. A. Advances in edible oleogel technologies—A decade in review. *Food Res. Int.* **97**, 307–317 (2017).
5. Oliveira, S. M. et al. Food additive manufacturing with lipid-based inks: Evaluation of phytosterol-lecithin oleogels. *J. Food Eng.* **341**, 111317 (2023).
6. Pinto, T. C. et al. Oleogel-based systems for the delivery of bioactive compounds in foods. *Gels* **7**(3), 86 (2021).
7. Wang, Z. et al. Multicomponent oleogels prepared with high- and low-molecular-weight oleogelators: Ethylcellulose and waxes. *Foods* **12**(16), 3093 (2023).
8. Wang, Z. et al. Oleogels prepared with low molecular weight gelators: Texture, rheology and sensory properties, a review. *Crit. Rev. Food Sci. Nutr.* **63**(23), 6069–6113 (2023).
9. Kavya, M. et al. Edible oleogels based on high molecular weight oleogelators and its prospects in food applications. *Crit. Rev. Food Sci. Nutr.* **64**(13), 4432–4455 (2024).
10. Cui, X. et al. Oleogels as animal fat and shortening replacers: Research advances and application challenges. *Food Rev. Int.* 1–22 (2022).
11. Silva, S. S. et al. Tailoring natural-based oleogels combining ethylcellulose and virgin coconut oil. *Polymers* **14**(12), 2473 (2022).
12. Patel, A. R. et al. Edible applications of shellac oleogels: spreads, chocolate paste and cakes. *Food Funct.* **5**(4), 645–652 (2014).
13. Puşcaş, A. et al. Oleogels in food: A review of current and potential applications. *Foods* **9**(1), 70 (2020).
14. Demirkesen, I. & Mert, B. Recent developments of oleogel utilizations in bakery products. *Crit. Rev. Food Sci. Nutr.* **60**(14), 2460–2479 (2020).
15. Chen, H. et al. An approach to manufacturing heat-stable and bloom-resistant chocolate by the combination of oleogel and sweeteners. *J. Food Eng.* **330**, 111064 (2022).
16. Garavaglia, J. et al. Grape seed oil compounds: Biological and chemical actions for health. *Nutr. Metab. Insights* **9**, NMI. S32910 (2016).
17. Jin, Q. et al. Techno-economic analysis of a grape pomace biorefinery: Production of seed oil, polyphenols, and biochar. *Food Bioprod. Process.* **127**, 139–151 (2021).
18. Movahed, S. & Ghavami, M. Comparative and identification of fatty acid composition of Iranian and importing grape seed oil. *Pajouhesh Sazandegi* (2007).
19. BaratianGhorghi, Z. et al. Changes in thermal, textural, color and microstructure properties of oleogel made from beeswax with grape seed oil under the effect of cooling rate and oleogelator concentration. *Res. Innov. Food Sci. Technol.* **11**(1), 43–54 (2022).
20. Fernandes, L. et al. Seed oils of ten traditional Portuguese grape varieties with interesting chemical and antioxidant properties. *Food Res. Int.* **50**(1), 161–166 (2013).
21. Shinagawa, F. B., Santana, F. C. D. & Mancini-Filho, J. Effect of cold pressed grape seed oil on rats' biochemical markers and inflammatory profile. *Rev. Nutr.* **28**, 65–76 (2015).
22. Rogers, M. A. et al. Edible oleogels in molecular gastronomy. *Int. J. Gastron. Food Sci.* **2**(1), 22–31 (2014).
23. Dassanayake, L. S. K., Kodali, D. R. & Ueno, S. Formation of oleogels based on edible lipid materials. *Curr. Opin. Colloid Interface Sci.* **16**(5), 432–439 (2011).
24. Yilmaz, F. & Dagdemir, E. The effects of beeswax coating on quality of Kashar cheese during ripening. *Int. J. Food Sci. Technol.* **47**(12), 2582–2589 (2012).
25. Dassanayake, L. S. K. et al. Physical properties of rice bran wax in bulk and organogels. *J. Am. Oil Chem. Soc.* **86**(12), 1163–1173 (2009).
26. Öğütcü, M., Arifoğlu, N. & Yılmaz, E. Storage stability of cod liver oil organogels formed with beeswax and carnauba wax. *Int. J. Food Sci. Technol.* **50**(2), 404–412 (2015).
27. Martins, A. J. et al. Beeswax organogels: Influence of gelator concentration and oil type in the gelation process. *Food Res. Int.* **84**, 170–179 (2016).
28. Yao, Y. et al. The Effect of cooling rate on the microstructure and macroscopic properties of rice bran wax oleogels. *J. Oleo Sci.* **70**(1), 135–143 (2021).

29. Giacomozzi, A. S. et al. Physical properties of monoglycerides oleogels modified by concentration, cooling rate, and high-intensity ultrasound. *J. Food Sci.* **84**(9), 2549–2561 (2019).
30. Jana, S. & Martini, S. Effect of high-intensity ultrasound and cooling rate on the crystallization behavior of beeswax in edible oils. *J. Agric. Food Chem.* **62**(41), 10192–10202 (2014).
31. Martini, S., Herrera, M. L. & Hartel, R. W. Effect of cooling rate on crystallization behavior of milk fat fraction/sunflower oil blends. *J. Am. Oil Chem. Soc.* **79**(11), 1055–1062 (2002).
32. Soltanizadeh, N. & Goli, S. A. H. Evaluating the effect of cooling rate and organogelator concentration on the textural properties of sesame oil oleogels and comparison with animal fat. *J. Food Sci. Technol. (Iran)* **16**(90), 1–14 (2019).
33. Tarone, A. G. et al. Influence of drying conditions on the gelling properties of the 7S and 11S soy protein fractions. *Food Bioprod. Process.* **91**(2), 111–120 (2013).
34. Anvari, M. & Chung, D. Effect of cooling–heating rate on sol-gel transformation of fish gelatin–gum arabic complex coacervate phase. *Int. J. Biol. Macromol.* **91**, 450–456 (2016).
35. Awad, T. S. et al. Effect of cooling and heating rates on polymorphic transformations and gelation of tripalmitin solid lipid nanoparticle (SLN) suspensions. *Food Biophys.* **3**(2), 155–162 (2008).
36. De la Peña-Gil, A. et al. Combined effect of shearing and cooling rate on the rheology of organogels developed by selected gelators. *Food Res. Int.* **93**, 52–65 (2017).
37. Moritaka, H., Takahashi, M. & Kubota, K. Effects of cooling rate and sodium chloride on polysaccharide gelation. *Food Sci. Technol. Res.* **13**(4), 345–350 (2007).
38. Toro-Vazquez, J. F. et al. Cooling rate effects on the microstructure, solid content, and rheological properties of organogels of amides derived from stearic and (R)-12-hydroxystearic acid in vegetable oil. *Langmuir* **29**(25), 7642–7654 (2013).
39. Toro-Vazquez, J. F. et al. Thermal and textural properties of organogels developed by candelilla wax in safflower oil. *J. Am. Oil Chem. Soc.* **84**(11), 989–1000 (2007).
40. Doan, C. D. et al. Internal and external factors affecting the crystallization, gelation and applicability of wax-based oleogels in food industry. *Innov. Food Sci. Emerg. Technol.* **45**, 42–52 (2018).
41. Domian, E., Mańko-Jurkowska, D. & Górska, A. Heat-induced gelation, rheology and stability of oil-in-water emulsions prepared with patatin-rich potato protein. *Food Bioprod. Process.* **139**, 144–156 (2023).
42. Felix, M. et al. Development of thermally processed bioactive pea protein gels: Evaluation of mechanical and antioxidant properties. *Food Bioprod. Process.* **101**, 74–83 (2017).
43. Ghorghi, Z. B. et al. Fabrication of novel hybrid gel based on beeswax oleogel: Application in the compound chocolate formulation. *Food Hydrocoll.* **140**, 108599 (2023).
44. Pottathara, Y. B. et al. Solidification of gelatine hydrogels by using a cryoplatform and its validation through CFD approaches. *Gels* **8**(6), 368 (2022).
45. Kobus, C. J. & Wedekind, G. L. An experimental investigation into forced, natural and combined forced and natural convective heat transfer from stationary isothermal circular disks. *Int. J. Heat Mass Transf.* **38**(18), 3329–3339 (1995).
46. Bergman, T. L. et al. *Fundamentals of Heat and Mass Transfer* (John Wiley & Sons, 2020).
47. Civan, F. & Sliepcevich, C. M. Efficient numerical solution for enthalpy formulation of conduction heat transfer with phase change. *Int. J. Heat Mass Transf.* **27**(8), 1428–1430 (1984).
48. Comini, G. & Lewis, R. W. A numerical solution of two-dimensional problems involving heat and mass transfer. *Int. J. Heat Mass Transf.* **19**(12), 1387–1392 (1976).
49. Pham, Q. T. A fast, unconditionally stable finite-difference scheme for heat conduction with phase change. *Int. J. Heat Mass Transf.* **28**(11), 2079–2084 (1985).
50. Poirier, D. & Salcudean, M. On Numerical methods used in mathematical modeling of phase change in liquid metals. *J. Heat Transf.* **110**(3), 562–570 (1988).
51. Al-Saadi, S. N. & Zhai, Z. Modeling phase change materials embedded in building enclosure: A review. *Renew. Sustain. Energy Rev.* **21**, 659–673 (2013).
52. Caggiano, A., Mankel, C. & Koenders, E. Reviewing theoretical and numerical models for PCM-embedded cementitious composites. *Buildings* **9**(1) (2019).
53. Baehr, H. D. & Stephan, K. Convective heat and mass transfer. In *Flows with Phase Change* (eds Baehr, H. D. & Stephan, K.) 443–543 (Springer Berlin Heidelberg, 2011).
54. Yang, H. & He, Y. Solving heat transfer problems with phase change via smoothed effective heat capacity and element-free Galerkin methods. *Int Commun Heat Mass Transf* **37**(4), 385–392 (2010).
55. Li, G., Oka, Y. & Furuya, M. Experimental and numerical study of stratification and solidification/melting behaviors. *Nucl Eng Des* **272**, 109–117 (2014).
56. Choudhari, C. M., Narkhede, B. E. & Mahajan, S. K. Modeling and simulation with experimental validation of temperature distribution during solidification process in sand casting. *Int J Comput Appl* **78**, 23–29 (2013).

Author contributions

Z.B.G.: Investigation, Formal Analysis, Methodology, Resources, Software, Validation, Writing – Original Draft Preparation; A.F.: Conceptualization, Methodology, Supervision, Validation, Writing – Review & Editing; S.Y.: Conceptualization, Funding Acquisition, Methodology, Supervision, Validation, Writing – Review & Editing; M.A.H.: Conceptualization, Methodology, Resources, Validation, Software, Writing – Review & Editing; A.S.D.: Investigation, Methodology, Software, Validation, Writing – Review & Editing; M.F.: Writing – Review & Editing; H.A.T.: Investigation, Methodology, Validation, Writing – Review & Editing.

Funding

The authors would like to acknowledge the Research Institute of FoodScience and Technology (RIFST), Iran for supporting the research grant.

Declarations

Competing interests

The authors declare no competing interests.

Consent for publication

All authors have read and agreed to the published version of themanuscript. All authors read and approved the final manuscript.

Additional information

Correspondence and requests for materials should be addressed to A.F. or S.Y.

Reprints and permissions information is available at www.nature.com/reprints.

Publisher's note Springer Nature remains neutral with regard to jurisdictional claims in published maps and institutional affiliations.